Nanoscale

Accepted Manuscript

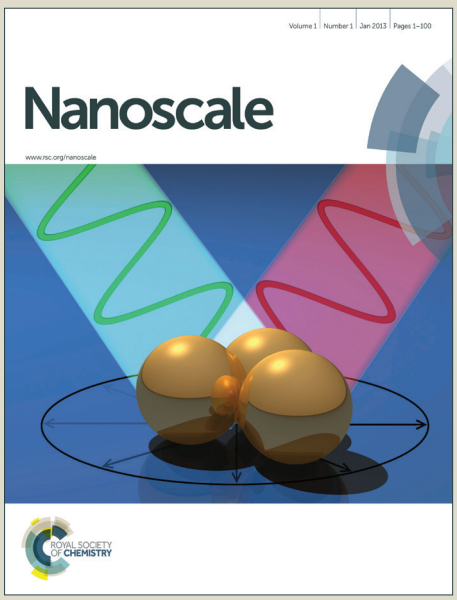

ROYAL SOCIETY OF CHEMISTRY

www.rsc.org/nanoscale

Nanoscale Paper

Electric field mediated non-volatile tuning magnetism at single-crystalline Fe/Pb($Mg_{1/3}Nb_{2/3}$)$_{0.7}Ti_{0.3}O_3$ interface

Chao Zhang,[a] Fenglong Wang,[a] Chunhui Dong,[a] Cunxu Gao,[a] Chenglong Jia,[a] Changjun Jiang*[a] and Desheng Xue*[a]

We report non-volatile electric-field control of magnetism modulation in Fe/Pb($Mg_{1/3}Nb_{2/3}$)$_{0.7}Ti_{0.3}O_3$ (PMN-PT) heterostructure by fabricating an epitaxial Fe layer on PMN-PT substrate using molecular beam epitaxy technique. The remnant magnetization with different electric field shows a non-symmetric *looplike* shape, which demonstrates a change of interfacial chemistry and a large magnetoelectric coupling in Fe/PMN-PT at room temperature to realize low loss multi-state memory under electric field. Fitting with the angular-dependence of in-plane magnetization reveals that the magnetoelectric effect is dominated by the direct electric-field-effect rather than the strain effect at the interface. The magnetoelectric effect and the induced surface anisotropy are found to be dependent on the Fe film thickness and linear with respect to the applied electric field.

Introduction

Multiferroic materials have two or more kinds of ferroic properties, such as ferroelectricity, ferromagnetism and ferroelasticity.[1-7] It is of great importance to understand and realize to manipulate the magnetism of multiferroic materials in terms of magnetoelectric (ME) effect. Due to a fast, low-power, energy efficient manner of ME effect,[8, 9] the multiferroic system could often be used to make sensors, multi-state memory, and other spintronics devices[10, 11]. So far, the electric-field control of magnetism has been observed experimentally in artificial ferromagnetic (FM)/ ferroelectric (FE) heterostructures[12-14] and intrinsically multiferroics, for instance $BiFeO_3$[15, 16]. However, in the single-phase multiferroics the

intrinsic coupling between polarization and magnetization at atomic scale is generally weak and at low temperature, which limit their practical applications. Aiming at a large technological impact, artificial FM/FE composites are designed to improve ME couplings, which progress are made in the electrical control of magnetic anisotropy[17], domain structure[14], spin polarization[18] or critical temperatures[19]. In composite system relying on the interfacial effect, the ME coupling can be classified according to its origin: (i) indirect strain-mediated coupling at FM/piezoelectric interfaces[20-25], (ii) indirect exchange-bias mediated coupling such at FM/$BiFeO_3$ interface[16, 26], (iii) and direct electric field effect including modulation of carrier density in the Fermi surface of FM layer[13, 27, 28], interfacial chemistry by ionic displacement FM/FE interfaces[29] and spin-charge screening[19]. Concerning atomic motion of metallic layer induced by an electric field, several studies have been reported to indicate an emergence of the metallic oxidation, which is found to be reversible interestingly[30-33]. For spin-charge screening effect, we would have an intrinsic linear ME coupling that is most pronounced in the vicinity of the FM/FE interface acting within the spin-diffusion length λ_m of the order of nanometers[34]. However, in spite of the tremendous research effort, the underlying physics behind ME interactions remains puzzling in many aspects. In this work, we clearly demonstrate a non-volatile electric field mediated ME interaction in an epitaxial Fe layer on $Pb(Mg_{1/3}Nb_{2/3})_{0.7}Ti_{0.3}O_3$ (PMN-PT) heterostructures. Such the charge-dominant interfacial ME effect is found evidence by the hysteresis *looplike* M_r-E curve and the linear relationship of surface anisotropy with applied gate-voltage.

Experimental

Single-crystalline Fe thin films with a thickness of about 30 nm are deposited on (011)-oriented PMN-PT single-crystalline substrates by molecular beam epitaxy (MBE). PMN-PT substrate is thermal cleaned at 500 ºC for 20 min before depositing Fe film. After lowering the temperature to room temperature without

any external electric field, Fe film is then started to grow on the PMN-PT at the rate of 1.4 Å/min. This treatment can make sure that Fe/PMN-PT sample at 0 kV/cm is unpoled state. Reflection high-energy electron diffraction (RHEED) indicates epitaxial growth of Fe layer along single PMN-PT substrate. Transmission electron microscopy (TEM, Tecnai TMG2F30) shows Fe crystal grows on the surface of [011] PMN-PT and clear lattice fringes are observed indicating single crystal cubic-Fe, as shown in Fig. 1 (a). The sketch of the sample and the measurement configuration is shown in figure 1(b). Pt layers are sputtered on both the top and bottom sides of the Fe/PMN-PT structure as electrodes by magnetron sputtering at room temperature. Cu wires are connected to the electrodes by adhesive tape and the electric field applied between the sample surfaces is controlled by a dc power supply Keithley 6517B. Polarization-electric field (*P*-*E*) characteristics are measured using a ferroelectric test system (Radiant, Precision Premier Ⅱ, USA). Magnetic properties are measured using a vibrating sample magnetometer (VSM, Microsence EV9). In order to obtain specified magnetic field angles a stepping motor controlled by the measuring software system of VSM is used to rotate the sample holder with accuracy of 0.5 degree.

Results and discussions

In order to investigate the magnetic anisotropy of the single crystal Fe, angle-remanent curves are measured under different electric field of 0 and 10 kV/cm, respectively. The sample is attached to a rotatable holder and M_r is measured every 5 from 0 to 360 degree. Before obtaining each data point, a saturation field of 800 Oe is first applied then reduced to zero to achieve a remanence state. Figure 1(c) illustrates the angular dependence of M_r under different electric field. Here, angle 0 degree is only a starting point in our measurement and the value of angle is a relative degree with sample's certain situation. Notice that angle 0 degree under different electric field is the same situation of the sample. The

0 kV/cm curve shows an overlay of two and four fold symmetric magnetic anisotropy. At 115 and 295 degree, the M_r reaches its minimum value, which implies the hard magnetizing axis; at 25 and 205 degree the M_r gets to its second minimum value, which suggests the second hard magnetizing axis. Applying a dc electric field 10 kV/cm, obvious change of M_r *vs* α is observed, which indicates turning magnetism of electric field. Note that peak position of the first and the second hard magnetizing axis is not changed. Electric field induced change in magnetic hysteresis loops is measured using the VSM. Figure 1(d) presents representative magnetic hysteresis loops measured along 25 and 115 degree the in-plane Fe/PMN-PT heterostructure under the application of different electric field across the PMN-PT single crystal substrate. The application of electric field could decrease the M_r and coercivity obviously at 25 degree, while the M_r and coercivity at 115 degree is increased.

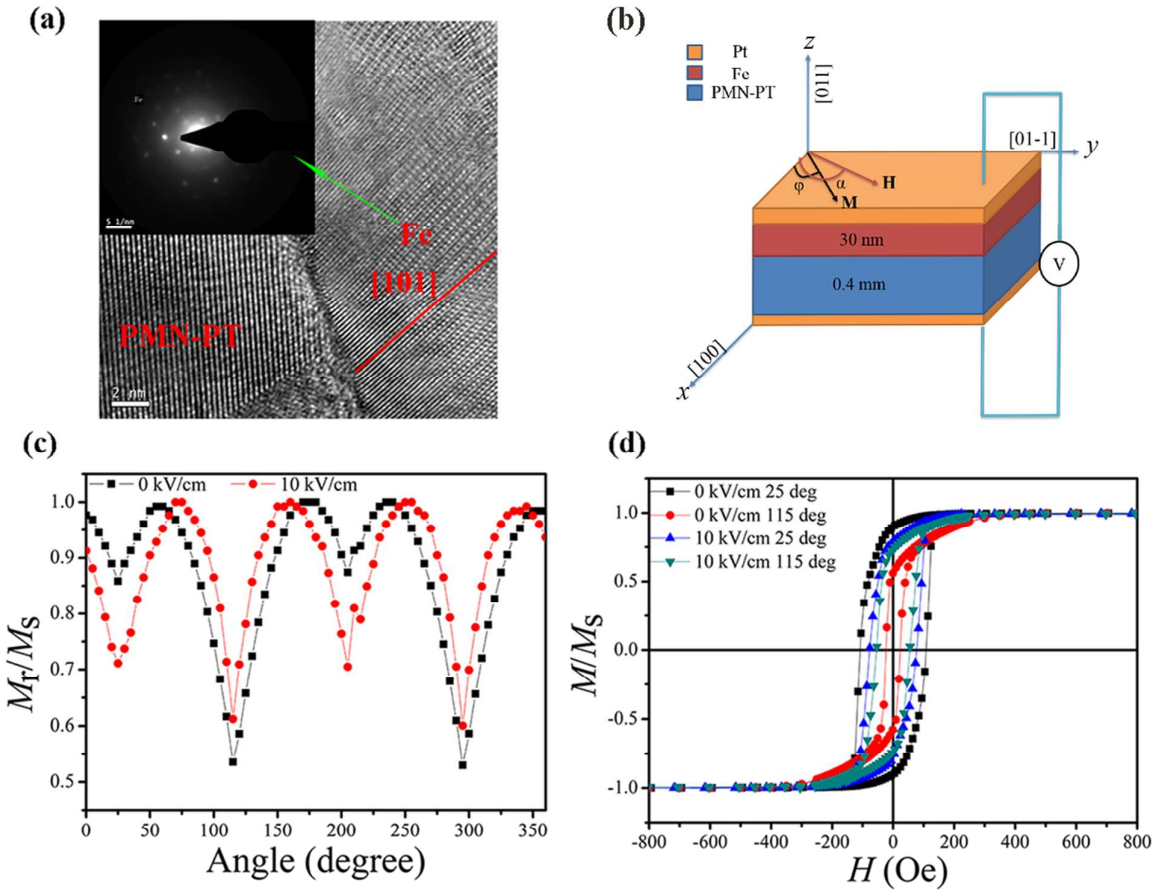

Figure 1. (a)TEM image of single-crystalline Fe /PMN-PT (b) Sketch of the single-crystalline Fe/PMN-PT multiferroic heterostructures and the VSM in-plane measurement configuration. (c) The remanent magnetization (M_r) versus (*vs*) angle (α) under 0 kV/cm and 10 kV/cm. (d) The hysteresis loop with different electric field along 25 degree and 115 degree, indicating the anisotropy changes.

For an insight into the possible interfacial ME interactions, M_r under different electric field E is measured at 25 and 115 degree, respectively. The value of M_r is obtained at zero fields after removing saturation field of 800 Oe. The M_r *vs* E curves at 25 and 115 degree is obtained (as shown in figure 2(a) and (b)), which shows *looplike* magnetization-electric field response. M_r at 25 degree is decreased with the increase of positive electric field, while increased with the electric field swept from 0 to -10 kV/cm. Note that M_r is almost unchanged at a negative electric field with the electric field swept from -10 kV/cm to 0 kV/cm. The curves at 115 degree shows similar difference between positive and negative electric field. In principle, the coexistence of strain and charge mediated ME coupling would be expected in our sample. For strain effect, in-plane magnetization would be controlled through biaxial stress originating from the piezoelectricity of PMN-PT substrate. In figure 2(c), strain-electric field (*S*-*E*) curves are measured at room temperature by a strain gauge (KFG-1-120-D17, KYOWA). From symmetry point of view, the standard "butterfly" *S*-*E* curve should result in a characteristic strain-mediated piezoelectric semi-butterfly like M_r-E curve. However, M_r-E curves in Fig. 2(a) and (b) show quite non-symmetric *looplike* shape, which implies that the strain effect does not play a key role in the interfacial ME effect. Therefore, the transposition of coupling phenomena should be considered with care. Taking that the surface charge screening length is less than 1 nm for typical FM metals, the pure charge-mediated ME coupling can thus be ignored in our Fe (30 nm) film as well. On the other hand, a new magnon-driven, strong ME effect would take an effect on Fe film with thickness over tens of nanometers[20]. By interfacing FM (Fe) with FE (PMN-PT), it triggers in the FM low-energy coherent magnetic excitations near the

interface, which builds up a spatially inhomogeneous (spiral) surface magnetic order, yields an intrinsic linear ME coupling that is most pronounced in the vicinity of the spin diffusion length (10 nm in Fe)[34,35]. Hence we expect that the spin-driven screening effect is a main factor in our system. However, note that non-symmetric M_r-E curves, especially the nearly unchanged M_r swept from -10 kV/cm to 0 kV/cm, there should be also existed interfacial chemistry by ionic displacement FM/FE interfaces. Such the emergence of oxidation induced by negative electric field at interface has been observed when single-crystalline Fe-based film deposited on oxide substrate such as $BaTiO_3$[30, 31], MgO[32, 33]. In order to quantitatively understand the contribution from these different types of ME interaction, we analyse further the change of magnetism under different electric field, which included magnetocrystalline anisotropy and interface anisotropy.

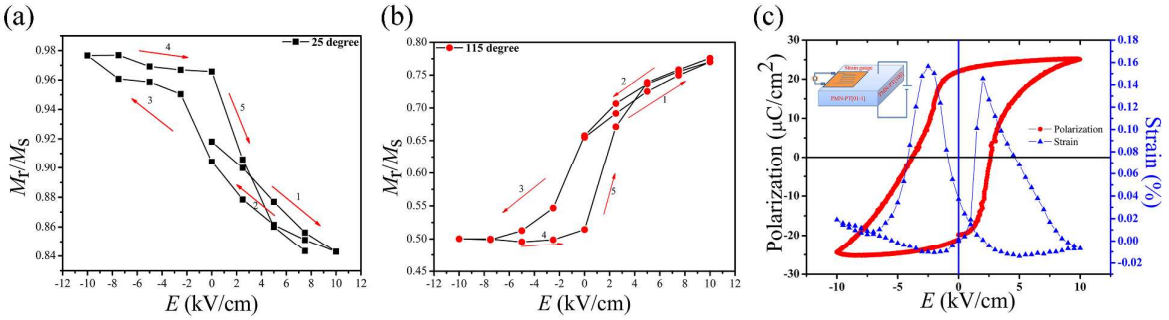

Figure 2. The M_r dependent with the electric field. (a) The applied field is along 25 degree (α=25°), and the number means the electric field swept process from 1 to 5. (b) The applied field is along 115 degree (α=115°). Loops have been normalized at saturation. (c) The P-E (red) and [100]-direction S-E (blue) curves of PMN-PT substrate (the insert graph shows the sketch of strain gauge measurement).

In order to demonstrate reversible magnetization process according to requirement of application, M_r with a pulse electric field is measured. Intermittent positive and negative electric field of 5 and 10 kV/cm is applied across the sample. The magnetic field is first set up to 800 Oe then reduced to zero. After

setting magnetic field to zero, the M_r was measured continuously. Figure 3(a) and (b) show electric-field-induced non-volatile magnetization switching under different pulse electric field. Stable and remarkable high/low magnetization states can be achieved by switching the polarity of electric field. The M_r with 10 kV/cm pulse electric field exhibits a fluctuation of about 20% of the zero electric field M_r. The reversible magnetization with pulse electric field can be used for four-state memory devices.

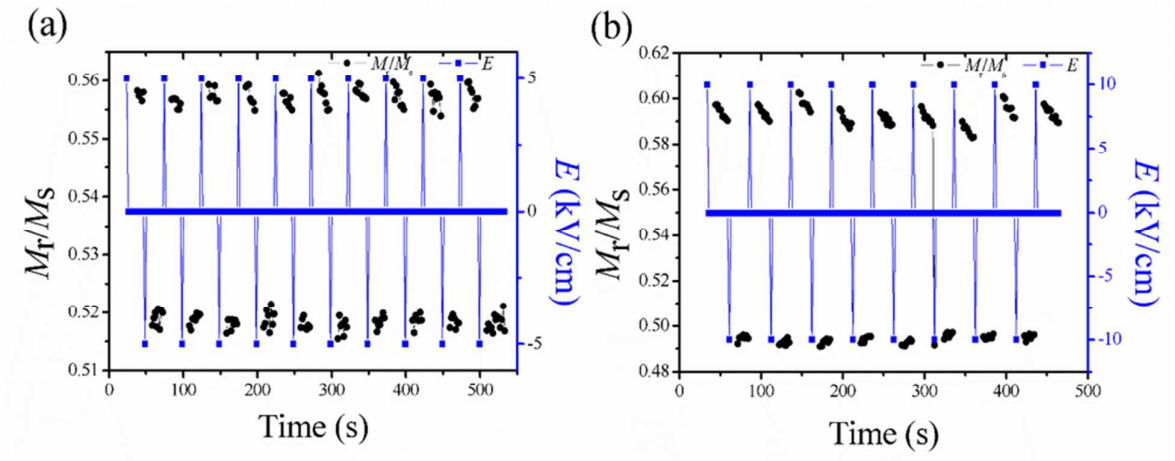

Figure 3.The M_r pulse-measure. (a) The alteration of M_r along 115 degree under 5 kV/cm pulse electric field. (b) The alteration of M_r along 115 degree under 10 kV/cm pulse electric field.

Based on above results, to explore turning magnetism of Fe/PMN-PT by electric field, the M_r as the function of angle with various positive electric fields is measured. Figure 4 (a) illustrates the angular dependence of M_r under different positive electric fields. In order to understand the alteration of anisotropy, we calculate the total energy according to Stoner-Wohlfarth model[36-38]. The total energy can be expressed as:

$$E_{tot} = E_{ani} + E_{charge} + E_{shape} + E_{zeeman} \quad (1)$$

where E_{ani} is the magnetocrystalline anisotropy energy, E_{charge} the surface energy, E_{shape} the demagnetizing energy, E_{zeeman} the Zeeman energy. The magneto-crystalline anisotropy which reflects the symmetry of

the crystal structure and is caused by the spin-orbit interaction is of particular importance. Such an anisotropy energy can be expressed using the direction cosine of the magnetization with respect to the [100] axes: α_1, α_2, and α_3. After considering the crystal symmetry, for a thin tetragonal magnetic film with arbitrary magnetization direction and addition uniaxial in-plane anisotropy, it reads,

$$\begin{aligned} E_{\text{ani}} = & -K_{\text{u}\perp}\cos^2\theta - K_{\text{u}//}\sin(\varphi-\varphi_{\text{u}})\sin^2\theta \\ & -\frac{1}{2}K_{1\perp}\cos^4\theta - \frac{1}{8}K_{1//}(3+\cos 4\varphi)\sin^4\theta \end{aligned} \qquad (2)$$

where $K_{\text{u}\perp}$ and $K_{1\perp}$ ($K_{\text{u}//}$ and $K_{1//}$) are the bulk out-of-plane (in-plane) uniaxial and cubic anisotropy due to the tetragonal distortion, respectively. φ_{u} denotes the angle of the easy axis of the uniaxial anisotropy with respect to the [100]-direction for a positive $K_{\text{u}//}$, as shown in figure 1(a). Therefore, the further total energy can be expressed as:

$$\begin{aligned} E_{\text{tot}} = & -K_{\text{u}\perp}\cos^2\theta - K_{\text{u}//}\sin(\varphi-\varphi_u)\sin^2\theta - \frac{1}{2}K_{1\perp}\cos^4\theta \\ & -\frac{1}{8}K_{1//}(3+\cos 4\varphi)\sin^4\theta + \frac{K_{\text{s}}(E)}{d}\cos^2\varphi\sin^2\theta \\ & +\frac{1}{2}\mu_0 M_{\text{s}}^2\cos^2\theta - \mu_0 M_{\text{s}} H\sin\theta\cos(\alpha-\varphi) \end{aligned} \qquad (3)$$

where d, $K_{\text{s}}(E)$ and M_{s} is the thickness, surface anisotropy, magnetization of the Fe film, respectively.

Considering to high saturated magnetization and large demagnetizing field, magnetic moment of Fe was lied in the film plane, which means $\theta = \frac{\pi}{2}$. M_{r} is achieved as the αdependence of the magnetization M_{r} which is satisfied with

$$M_{\text{r}} = M_{\text{s}}\cos(\alpha-\varphi) \qquad (4)$$

The equilibrium conditions:

$$\frac{\partial E_{tot}}{\partial\varphi} = 0, \frac{\partial^2 E_{\text{tot}}}{\partial\varphi^2} = 0 \qquad (5)$$

Assuming that α and φ has a simple liner function: $\alpha=\varphi+\varphi_0$, and a differential constant m, hence we obtained:

$$\frac{M_r}{M_s}=-\frac{2K_{1//}}{\mu_0 M_s H}\cos 4(\alpha-\varphi_0)+\frac{2K_s(E)}{\mu_0 M_s Hd}\cos 2(\alpha-\varphi_0)$$
$$-\frac{K_{u//}}{\mu_0 M_s H}\sin(\alpha-\varphi_0-\varphi_u)+m \qquad (6)$$

Based on formula (6), fitted curves of M_r *vs* α is showed in figure 4(a). In order to obtain electric field controlled magnetism, the change of cubic magnetocrystalline anisotropy $\Delta K_{1//}$ and surface anisotropy ΔK_s comparing with those of unpolarized sample are obtained, as shown in figure 4(b). The change of magnetocrystalline anisotropy $\Delta K_{1//}$ is almost zero, which indicated unchanged Fe crystal structure and a little of strain effect under electric field. The surface anisotropy is controlled dramatically by positive electric field and almost unchanged (note the difference with that of unpolarized sample) under negative electric field, which indicated that oxide layer under negative field changed interface structure and charge effect under positive field induced the linear change of surface anisotropy.

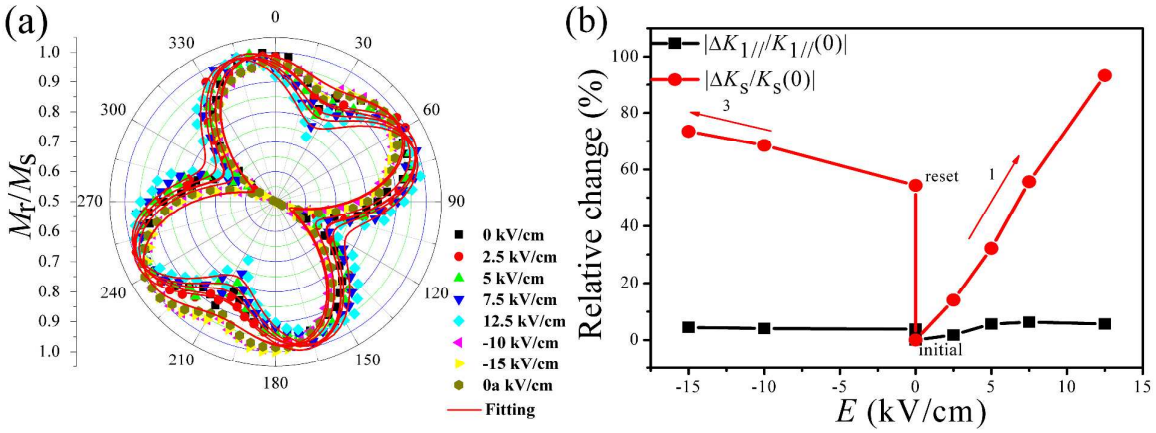

Figure 4.The M_r *vs* α and fitting anisotropy change of 30 nm thickness Fe /PMN-PT. (a) The polar graph of M_r (scatter) and the fitting curve (line). (b) The relative change of magnetocrystalline and surface anisotropy by fitting dependence with electric fields. The initial 0 kV/cm point means the sample is

unpolarized, while the reset 0 kV/cm point means the sample is polarized with negative electric field then remove electric field.

Based on above discussion, interface anisotropy should be enhanced with decreasing the thickness of FM layer. In order to further investigate electric field mediated ME coupling effects in Fe/PMN-PT, the angular dependence of M_r in 15 nm Fe sample were also acquired with different applied electric fields. Based on formula (6), fitted curves of M_r *vs* α is showed in figure 5(a). Surface anisotropy in 15 nm sample is linear relationship to electric field comparing with that of 30 nm Fe film, as shown in Fig 5 (b). In addition, our results demonstrate the increase of surface anisotropy and almost unchanged of magnetocrystalline anisotropy with decreasing thickness of Fe film, which further illustrate the dominant of interface spin-charge screening effect mediated ME coupling comparing with strain effect. Due to the existence of spin-charge screening in the interface of Fe/PMN-PT, we work out theoretically a mechanism for ME coupling driven by a buildup of an interfacial spiral spin density in FM/FE composites[34]. Due to the large spin-diffusion length in FM metals, ME effects may have substantial influence on FM layers with thickness over tens of nanometers. In addition, spin-charge mediated surface anisotropy is linearly induced by electric field, which also shows the thickness dependence in FM layer. Anyway, our experimental results show ME effects of charge mediated spin charge screening and interfacial chemistry by ionic displacement FM/FE interfaces.

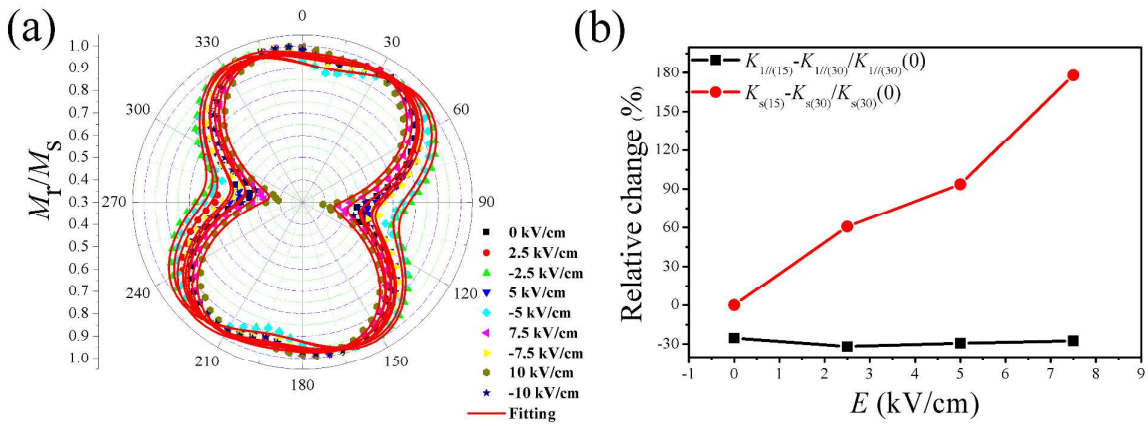

Figure 5.The M_r *vs* α and fitting anisotropy change of 15 nm thickness Fe /PMN-PT. (a) The polar graph of M_r (scatter) and the fitting curve (line). (b) The relative change of magnetocrystalline and surface anisotropy comparing with that of 30 nm Fe film by fitting dependence with electric fields.

Conclusions

In summary, we obtain a non-volatile magnetism manipulation with electric field at single-crystalline Fe/PMN-PT composite, which is induced by spin-charge screening effect and interfacial chemistry by ionic displacement of Fe layer in the interface. Moreover, the surface anisotropy by fitting the M_r vs α curve under different electric field is obtained and linear change under positive electric field is observed due to spin-charge screening mediated magnetic surface anisotropy. The reversible magnetization process is obtained by pulse electric field, which is desirable for the application of low energy ME devices such as four-state memory.

Acknowledgments

This work is supported by National Basic Research Program of China (Grant No. 2012CB933101), the National Natural Science Foundation of China (Grant No. 11474138, 11374131, and 11274147), the Program for Changjiang Scholars and Innovative Research Team

in University (No. IRT1251), and the Fundamental Research Funds for the Central Universities (No. 2022013zrct01).

Notes and references

[a] Key Laboratory for Magnetism and Magnetic Materials of MOE, Lanzhou University, Lanzhou 730000, People's Republic of China. Fax: 8914160, Tel: 8914160, E-mail: jiangchj@lzu.edu.cn & xueds@lzu.edu.cn

1. N. X. Sun and G. Srinivasan, *Spin*, 2012, **02**, 1240004.
2. C. A. Vaz, *J. Phys.: Condens. Matter*, 2012, **24**, 333201.
3. N. A. Spaldin, S. W. Cheong and R. Ramesh, *Phys. Today*, 2010, **63**, 38-43.
4. C.-W. Nan, M. I. Bichurin, S. Dong, D. Viehland and G. Srinivasan, *J. Appl. Phys.*, 2008, **103**, 031101.
5. T. Nan, Z. Zhou, M. Liu, X. Yang, Y. Gao, B. A. Assaf, H. Lin, S. Velu, X. Wang, H. Luo, J. Chen, S. Akhtar, E. Hu, R. Rajiv, K. Krishnan, S. Sreedhar, D. Heiman, B. M. Howe, G. J. Brown and N. X. Sun, *Sci. Rep.*, 2014, **4**, 3688.
6. Y.-L. Zhao, Q.-P. Chen, Y.-G. Zhao, L. Pan and Y. Sun, *Appl. Phys. Lett.*, 2013, **103**, 082905.
7. S.-E. Park and T. R. Shrout, *J. Appl. Phys.*, 1997, **82**, 1804.
8. S. Zhang, Y. Zhao, X. Xiao, Y. Wu, S. Rizwan, L. Yang, P. Li, J. Wang, M. Zhu, H. Zhang, X. Jin and X. Han, *Sci. Rep.*, 2014, **4**, 3727.
9. X. Marti, I. Fina, C. Frontera, J. Liu, P. Wadley, Q. He, R. J. Paull, J. D. Clarkson, J. Kudrnovsky, I. Turek, J. Kunes, D. Yi, J. H. Chu, C. T. Nelson, L. You, E. Arenholz, S. Salahuddin, J. Fontcuberta, T. Jungwirth and R. Ramesh, *Nat. Mater.*, 2014, **13**, 367-374.
10. I. Žutić, J. Fabian and S. D. Sarma, *Rev. Mod. Phys.*, 2004, **76**, 323.
11. K. Roy, S. Bandyopadhyay and J. Atulasimha, *Appl. Phys. Lett.*, 2011, **99**, 063108.
12. M. Liu, S. Li, O. Obi, J. Lou, S. Rand and N. X. Sun, *Appl. Phys. Lett.*, 2011, **98**, 222509.
13. M. Weisheit, S. Fahler, A. Marty, Y. Souche, C. Poinsignon and D. Givord, *Science*, 2007, **315**, 349-351.
14. S. Zhang, Y. G. Zhao, P. S. Li, J. J. Yang, S. Rizwan, J. X. Zhang, J. Seidel, T. L. Qu, Y. J. Yang, Z. L. Luo, Q. He, T. Zou, Q. P. Chen, J. W. Wang, L. F. Yang, Y. Sun, Y. Z. Wu, X. Xiao, X. F. Jin, J. Huang, C. Gao, X. F. Han and R. Ramesh, *Phys. Rev. Lett.*, 2012, **108**, 137203.
15. S. M. Wu, S. A. Cybart, D. Yi, J. M. Parker, R. Ramesh and R. C. Dynes, *Phys. Rev. Lett.*, 2013, **110**, 067202.
16. S. M. Wu, S. A. Cybart, P. Yu, M. D. Rossell, J. X. Zhang, R. Ramesh and R. C. Dynes, *Nat. Mater.*, 2010, **9**, 756-761.
17. M. Liu, S. Li, Z. Zhou, S. Beguhn, J. Lou, F. Xu, T. Jian Lu and N. X. Sun, *J. Appl. Phys.*, 2012, **112**, 063917.
18. M. Liu, J. Hoffman, J. Wang, J. Zhang, B. Nelson-Cheeseman and A. Bhattacharya, *Sci. Rep.*, 2013, **3**, 1876.
19. C.-G. Duan, J. Velev, R. Sabirianov, Z. Zhu, J. Chu, S. Jaswal and E. Tsymbal, *Phys. Rev. Lett.*, 2008, **101**, 137201.
20. N. Jedrecy, H. J. von Bardeleben, V. Badjeck, D. Demaille, D. Stanescu, H. Magnan and A. Barbier, *Phys. Rev. B*, 2013, **88**, 121409.
21. N. Li, M. Liu, Z. Zhou, N. X. Sun, D. V. B. Murthy, G. Srinivasan, T. M. Klein, V. M. Petrov and A. Gupta, *Appl. Phys. Lett.*, 2011, **99**, 192502.
22. M. Liu, O. Obi, J. Lou, Y. Chen, Z. Cai, S. Stoute, M. Espanol, M. Lew, X. Situ, K. S. Ziemer, V. G. Harris and N. X. Sun, *Adv. Func. Mater.*, 2009, **19**, 1826-1831.
23. N. A. Pertsev, H. Kohlstedt and R. Knöchel, *Phys. Rev. B*, 2011, **84**, 014423.
24. L. Shu, Z. Li, J. Ma, Y. Gao, L. Gu, Y. Shen, Y. Lin and C. W. Nan, *Appl. Phys. Lett.*, 2012, **100**, 022405.
25. M. Liu, Z. Zhou, T. Nan, B. M. Howe, G. J. Brown and N. X. Sun, *Adv. Mater.*, 2013, **25**, 1435-1439.
26. V. Laukhin, V. Skumryev, X. Martí, D. Hrabovsky, F. Sánchez, M. García-Cuenca, C. Ferrater, M. Varela, U. Lüders, J. Bobo and J. Fontcuberta, *Phys. Rev. Lett.*, 2006, **97**, 227201.
27. H. J. A. Molegraaf, J. Hoffman, C. A. F. Vaz, S. Gariglio, D. van der Marel, C. H. Ahn and J.-M. Triscone, *Adv. Mater.*, 2009, **21**, 3470-3474.

28. Y. W. Yin, J. D. Burton, Y. M. Kim, A. Y. Borisevich, S. J. Pennycook, S. M. Yang, T. W. Noh, A. Gruverman, X. G. Li, E. Y. Tsymbal and Q. Li, *Nat. Mater.*, 2013, **12**, 397-402.
29. C.-G. Duan, S. Jaswal and E. Tsymbal, *Phys. Rev. Lett.*, 2006, **97**, 047201.
30. G. Radaelli, D. Petti, E. Plekhanov, I. Fina, P. Torelli, B. R. Salles, M. Cantoni, C. Rinaldi, D. Gutierrez, G. Panaccione, M. Varela, S. Picozzi, J. Fontcuberta and R. Bertacco, *Nat. Commun.*, 2014, **5**, 3404.
31. S. Couet, M. Bisht, M. Trekels, M. Menghini, C. Petermann, M. J. Van Bael, J.-P. Locquet, R. Rüffer, A. Vantomme and K. Temst, *Adv. Func. Mater.*, 2014, **24**, 71-76.
32. K. Leistner, J. Wunderwald, N. Lange, S. Oswald, M. Richter, H. Zhang, L. Schultz and S. Fähler, *Phys. Rev. B*, 2013, **87**, 224411.
33. F. Bonell, Y. T. Takahashi, D. D. Lam, S. Yoshida, Y. Shiota, S. Miwa, T. Nakamura and Y. Suzuki, *Appl. Phys. Lett.*, 2013, **102**, 152401.
34. C. L. Jia, T. L. Wei, C. J. Jiang, D. S. Xue, A. Sukhov and J. Berakdar, *Phys. Rev. B*, 2014, **90**, 054423.
35. J. Bass and W. P. Pratt, *J. Phys.: Condens. Matter*, 2007, **19**, 183201.
36. E. C. Stoner and E. P. Wohlfarth, *Phil. Trans. R. Soc. Lond. A*, 1948, **240**, 599-642.
37. C. Tannous and J. Gieraltowski, *Eur. J. Phys.*, 2008, **29**, 475-487.
38. D. L. Atherton and J. R. Beattie, *IEEE Trans. Magn.*, 1990, **26**, 3059-3063.